Impact of deposition pressure and two-step growth technique on the photoresponsivity enhancement of polycrystalline BaSi2 films formed by sputtering

doi: 10.7567/1882-0786/aafc70

Impact of deposition pressure and two-step growth technique on the photoresponsivity enhancement of polycrystalline $BaSi_2$ films formed by sputtering

Satoshi Matsuno[1], Taira Nemoto[1], Masami Mesuda[2], Hideto Kuramochi[2], Kaoru Toko[1], Takashi Suemasu[1]

[1]Institute of Applied Physics, University of Tsukuba, Ibaraki 305-8573, Japan

[2]Tosoh Corporation, Advanced Materials Research Laboratory, Kanagawa 252-1123, Japan

We investigate the influence of deposition pressure in the range 0.25–1.0 Pa on the photoresponsivity of 200-nm-thick $BaSi_2$ films grown by sputtering at 600 °C. $BaSi_2$ films formed at 0.8 Pa exhibit a high photoresponsivity. The deposited Ba-to-Si atomic ratio depends significantly on the sputtering pressure. That's why the pressure influences the photoresponsivity. $BaSi_2$ films grown by a two-step growth technique show much higher photoresponsivity almost equivalent to those grown by molecular beam epitaxy. The photoresponsivity reaches 0.75 A/W at 2.0 eV at a bias voltage of 0.5 V applied between the top and bottom electrode.

Wafer-based silicon (Si) solar cells dominate the market share, and their conversion efficiency (η) has exceeded 26%.[1] The achieved η is already close to the theoretical limit.[2] Under these circumstances, various thin-film solar cell materials have been studied.[3-6] Among these materials, we have paid special attention to semiconducting barium disilicide ($BaSi_2$). Solar cell materials should be safe, stable, and earth-abundant like Si. In addition, a large absorption coefficient (α), a suitable band gap, and superior minority-carrier properties are important for solar cell materials to achieve a high η. $BaSi_2$ has all these properties.[7,8] It has a band gap of 1.3 eV,[9] a large α of 3×10^4 cm^{-1} at 1.5 eV,[10-12] inactive grain boundaries,[13] and a large minority-carrier lifetime ($\tau \sim 10$ μs).[14,15] We have achieved η approaching 10% in p-$BaSi_2$/n-Si heterojunction solar cells[16,17] and recently demonstrated the operation of $BaSi_2$ homojunction solar cells.[18] A lot of studies have been carried out thus far on $BaSi_2$ epitaxial films grown by molecular beam epitaxy (MBE). MBE is, however, not a practical method to form films on large-area substrates. On the other hand, vacuum evaporation and sputtering are more feasible methods than MBE. $BaSi_2$ films formed by vacuum evaporation using $BaSi_2$ granules have been reported by Usami and Hara *et al.*,[19–22] and they achieved a high carrier lifetime of 4.8 μs in the films grown at 500 °C[21] and p-$BaSi_2$/n-Si heterojunction solar cells.[22] Sputtering is another large-area thin-film growth technique, and has been used to from semiconducting silicides such as β-$FeSi_2$ and Mg_2Si.[23,24] Previously, we have significantly improved photoresponsivities of $BaSi_2$ films formed by sputtering on a Si(111) substrate at 600 °C when the sputtering pressure (P) was set to 0.25 Pa.[25] However, the influence of the P on the photoresponse properties of $BaSi_2$ films has yet to be investigated. The Ba-to-Si atomic ratio of deposited films changes depending on the P during sputtering,[25] unlike in the Mg_2Si films by sputtering.[24] In the case of $BaSi_2$ films grown by MBE, the deviation of a Ba-to-Si atomic ratio from stoichiometry affects significantly their electrical and optical properties.[26] Therefore, it is of great importance to clarify the influence of P on the properties of $BaSi_2$ films formed by sputtering.

In this study, we grew $BaSi_2$ films at difference P values in the range 0.25–1.0 Pa for the growth of 200-nm-thick $BaSi_2$ films at a substrate temperature of 600 °C, and studied the influence of P on their photoresponsivities. We also examined the effect of two-step growth technique for $BaSi_2$ films, that is, the Ba atomic ratio was set higher in the 1st step than in the 2nd step. This is to flatten the Ba-to-Si atomic ratio especially around the $BaSi_2$/Si interface, where the Si atomic ratio is likely to be in excess because of the diffusion of Si atoms from the Si substrate. Similar technique has been used to control the crystal orientation of $BaSi_2$ films grown by MBE[27] and by vacuum evaporation,[28] other semiconducting silicides.[29] By using this technique, the photoresponsivity was significantly enhanced to the extent that it reaches a value as high as those of MBE-grown $BaSi_2$ films.

We used helicon-wave excited plasma (HWP, ULVAC MB00-1040) sputtering with a 2-inch-diameter polycrystalline stoichiometric $BaSi_2$ target (Tosoh). Details of the sample preparation are summarized in Table I. The deposited Ba-to-Si atomic ratio was in excess of Si when only the $BaSi_2$ target was sputtered.[25] Thereby, we added three plate-like Ba sources (1.0 × 1.0 cm^2) on the $BaSi_2$ target to achieve the formation of $BaSi_2$ films.[25] In this work, first, we fabricated approximately 200-nm-thick $BaSi_2$ films (samples A1-A4) on a heated n-Si (111) substrate at 600 °C by sputtering. The sputtering pressure of Ar was set at 0.25, 0.4, 0.8, and 1.0 Pa, respectively, followed by a 3-nm-thick amorphous Si capping layer to prevent oxidation of the sample surface.[30] In the second experiment, we formed $BaSi_2$ films (sample A5) by a two-step growth method, wherein approximately a 10-nm-thick layer was formed at 500 °C and P = 1.0 Pa, followed by the formation of overlayers at 600 °C and P = 0.5 Pa. The flow rate of Ar was set to 10 sccm, and the radio-frequency power was set to 100 W. Raman spectroscopy (JASCO NRS-5100) using a frequency-doubled neodymium-doped-yttrium–aluminum–garnet (Nd:YAG) laser (532 nm, 5.1 mW) and grazing-incidence (GI) 2θ X-ray diffraction (XRD) with Cu-Kα radiation (Rigaku SmartLab) and were used to characterize the crystalline quality of the grown layers. N^+-type Si (111) (resistivity ρ < 0.01 Ωcm) substrates were used for the

74 photoresponsivity measurement to provide a negligible contribution of photogenerated carriers
75 in the n^+-Si substrate. Indium–tin oxide (ITO) surface electrodes with thicknesses of 80 nm and
76 diameter of 1 mm and Al rear electrodes were fabricated by sputtering. The photoresponse
77 spectra were acquired by a lock-in technique using a xenon lamp with a single monochromator
78 with a focal length of 25 cm (Bunko Keiki SM-1700A and RU-60N). The light intensity of the
79 lamp was calibrated using a pyroelectric sensor (Melles Griot 13PEM001/J). We used a high ρ
80 n-type Si (111) (ρ > 1000 Ωcm) substrate for the Hall measurement. All the measurement was
81 performed at room temperature (RT). The Ba-to-Si atomic ratio of samples deposited at RT was
82 measured by Rutherford backscattering spectrometry (RBS).[25)]

83 Figure 1 shows GI-XRD patterns of samples A1-A5. For reference, the calculated
84 diffraction pattern of the orthorhombic $BaSi_2$ is also shown. All of the observed diffraction
85 peaks are assigned to $BaSi_2$, showing that $BaSi_2$ films were grown. There is not so much
86 difference in the diffraction peaks among samples.

87 Figure 2 shows the Raman spectra of all these samples. The Raman lines originate
88 from Si tetrahedra with T_h symmetry in the lattice of $BaSi_2$. Identification of Raman lines is
89 given in Ref. 31. The transverse optical phonon line of Si (Si_{TO}) was observed in samples A1
90 and A2, sputtered at P = 0.25 and 0.4 Pa, respectively. Considering that the absorption
91 coefficient (α) of $BaSi_2$ at a wavelength of 532 nm is $\alpha = 3 \times 10^5$ cm^{-1},[11)] the penetration depth
92 of the laser light was limited to around $1/\alpha \times 3 \sim 0.1$ μm. This value is smaller than the layer
93 thickness of $BaSi_2$. Hence the Si_{TO} signal in samples A1 and A2 is interpreted to originate from
94 crystalline Si included in the $BaSi_2$ film. Similar Si_{TO} signals were detected in MBE-grown
95 $BaSi_2$ films when the deposited Si atomic ratio was high, being in excess of Si from
96 stoichiometry.[26,32)]

97 Figure 3(a) shows Ba (red) and Si (black) atomic ratios as a function of P for the
98 samples deposited at RT without an additional Ba source (dotted line) and those with one Ba
99 source on the $BaSi_2$ target (solid lines), measured by RBS.[25)] With decreasing P, the Si atomic

ratio is increased. Si atoms are also diffused from the heated Si substrate into the grown layer.[26] Therefore, it is reasonable to consider that the excess Si atoms exist in the form of crystalline Si in the $BaSi_2$ layers when $P = 0.25$ and 0.4 Pa. Here, we discuss why the Ba-to-Si atomic ratio depends on P. Figure 3(b) shows the experimentally obtained P dependence of deposition rate of sputtered films when the substrate temperature was set at RT to prevent the diffusion of Si atoms from the Si substrate.[25] The increase of P has both positive and negative contributions to the deposition rate due to the increase of both the sputtering yield and the scattering degree between Ar and sputtered particles. The fact that the deposition rate decreased as the P increased suggests that the latter effect appeared significant. The arrival rate, thereby the atomic ratio of sputtered films, is sensitive to the ratios of atomic numbers between the sputtered atoms (Si and Ba) and the sputtering gas molecules (Ar).[33] The atomic weight between Ba, Ar, and Si is in the order $M_{Ba} >> M_{Ar} > M_{Si}$, meaning that the effect of scattering by Ar atoms is more significant on Si atoms than Ba atoms. That's why the atomic ratio of Si decreased with increasing P in Fig. 3(a). A larger atomic ratio of Si in the low P region than stoichiometry means that the sputtering yield of Si (Y_{Si}) is more than Ba (Y_{Ba}) from a $BaSi_2$ target, whereas Y_{Si} is smaller than Y_{Ba} ($Y_{Si}/Y_{Ba} \sim 0.5$) as far as Si and Ba bulks are concerned.[34] We thus speculate that it has something to do with the fact that Ba atoms in the $BaSi_2$ bulk exist in the form of positively charged ions, while Si tetrahedra (Si_4) are negatively charged.[35]

Figure 4(a) shows the photoresponse spectra of samples A1-A4, sputtered at various P values. The bias voltage (V_{bias}) of 0.5 V was applied to the bottom electrode with respect to the front ITO electrode to extract the photogenerated holes in the n-type $BaSi_2$ films into the ITO electrode. The photoresponsivities of all the samples rapidly increased with V_{bias} for photon energies larger than the band gap of $BaSi_2$ (~1.3 eV). Hence, the spectrum is derived from photogenerated carriers in the $BaSi_2$ films. The photoresponsivity was drastically changed depending on P, and reached a maximum of 0.29 A/W at 2.3 eV for sample A3, sputtered at P = 0.8 Pa. This result means that the Ba-to-Si atomic ratio of the $BaSi_2$ film in sample A3 is close

to stoichiometry. However, the Si atomic ratio in the sputtered film around the $BaSi_2$/Si interface is considered to be in excess of Si due to the diffusion of Si atoms from the Si substrate. This was confirmed in MBE-grown $BaSi_2$ films by RBS.[26] According to a supercell approach based on first-principle density functional theory by Kumar *et al.*,[35] Si vacancies are most likely to emerge in $BaSi_2$ regardless in a Si-rich or Ba-rich condition, generating localized states within the band gap, and degrading the photoresponsivity. We therefore attempted to decrease the Si atomic ratio in the $BaSi_2$ film around the $BaSi_2$/Si interface by a two-step growth technique, wherein the Ba atomic ratio was set higher in the 1st step (P = 1.0 Pa) than in the 2nd step (P = 0.5 Pa). Figure 4(b) shows the photoresponse spectrum of sample A5, fabricated by the two-step method, and sample A3 (P = 0.8 Pa). The photoresponsivity further increased in sample A5 compared to sample A3; the photoresponsivity reached 0.75 A/W at 2.0 eV at V_{bias}=0.5 V. This value is almost equivalent to those of $BaSi_2$ epitaxial films grown by MBE.[26] We attribute this photoresponsivity enhancement to the Ba-to-Si atomic ratio in the $BaSi_2$ film in sample A5 being more close to stoichiometry on the whole than those in other samples. As shown in Figs. 1 and 2, we cannot see a pronounced difference in crystalline quality of $BaSi_2$ films between sample A5 and others. Regarding the electrical properties of grown films, there was also not so much difference between samples. The electron concentration was of the order of 10^{16} cm^{-3} at RT and the mobility was in the range 900–1000 cm^2/Vs, similar to undoped n-$BaSi_2$ epitaxial films grown by MBE.[9] We speculate that small barrier heights at grain boundaries (GBs) in $BaSi_2$[36] may not deteriorate the electron transport across GBs, resulting in such a large mobility even in polycrystalline $BaSi_2$ films. On the basis of these results, we conclude that sputtering is a promising fabrication method for $BaSi_2$ films.

In summary, we formed 200-nm-thick $BaSi_2$ films on Si(111) substrates by sputtering and investigated the influence of deposition pressure on their photoresponsivities. The photoresponsivity changed significantly on P as observed in those by MBE, and reached a maximum of 0.29 A/W at 2.3 eV at V_{bias} = 0.5 V when P = 0.8 Pa. The photoresponsivity was

further increased in $BaSi_2$ films prepared by a two-step growth technique; increasing up to 0.75 A/W at 2.0 eV at V_{bias} = 0.5 V. This value was equivalent to those of $BaSi_2$ epitaxial films by MBE.

Acknowledgments

This study was financially supported by JSPS KAKENHI Grant Numbers 17K18865 and 18H03767 and JST MIRAI.

1) K. Yoshikawa, H. Kawasaki, W. Yoshida, T. Irie, K. Konishi, K. Nakano, T. Uto, D. Adachi, M. Kanematsu, H. Uzu, and K. Yamamoto, Nat. Energy **2**, 17032 (2017).
2) W. Shockley and H. J. Queisser, J. Appl. Phys. **32**, 510 (1961).
3) P. Jackson, R. Wuerz, D. Hariskos, E. Lotter, W. Witte, and M. Powalla, Phys. Status Solidi RL **10**, 583 (2016).
4) X. Wu, Sol. Energy **77**, 803 (2004).
5) J. Burschka, N. Pellet, S.-J. Moon, R. Humphry-Baker, P. Gao, M. K. Nazeeruddin, and M. Grätzel, Nature **499**, 316 (2013).
6) W. S. Yang, J. H. Noh, N. J. Jeon, Y. C. Kim, S. Ryu, J. Seo, and S. I. Seok, Science **348**, 1234 (2015).
7) T. Suemasu, Jpn. J. Appl. Phys. **54**, 07JA01 (2015).
8) T. Suemasu and N. Usami, J. Phys. D: Appl. Phys. **50**, 023001 (2017).
9) K. Morita, Y. Inomata, and T. Suemasu, Thin Solid Films **508**, 363 (2006).
10) D. B. Migas, V. L. Shaposhnikov, and V. E. Borisenko, Phys. Status Solidi B **244**, 2611 (2007).
11) K. Toh, T. Saito, and T. Suemasu, Jpn. J. Appl. Phys. **50**, 068001 (2011).
12) M. Kumar, N. Umezawa, and M. Imai, Appl. Phys. Express **7**, 071203 (2014).
13) M. Baba, M. Kohyama, and T. Suemasu, J. Appl. Phys. **120**, 085311 (2016).
14) K. O. Hara, N. Usami, K. Toh, M. Baba, K. Toko, and T. Suemasu, J. Appl. Phys. **112**, 083108 (2012).
15) K. O. Hara, N. Usami, K. Nakamura, R. Takabe, M. Baba, K. Toko, and T. Suemasu, Appl. Phys. Express **6**, 112302 (2013).
16) S. Yachi, R. Takabe, K. Toko, and T. Suemasu, Appl. Phys. Lett. **109**, 072103 (2016).
17) T. Deng, T. Sato, Z. Xu, R. Takabe, S. Yachi, Y. Yamashita, K. Toko, and T. Suemasu, Appl. Phys. Express **11**, 062301 (2018).
18) K. Kodama, K. Toko, and T. Suemasu, Jpn. J. Appl. Phys. **57**, 050310 (2018).
19) K. O. Hara, Y. Nakagawa, T. Suemasu, and N. Usami, J. Appl. Phys. **54**, 07JE02 (2015).
20) K. O. Hara, C. T. Trinh, K. Arimoto, J. Yamanaka, K. Nakagawa, Y. Kurokawa, T. Suemasu, and N. Usami, J. Appl. Phys. **120**, 045103 (2016).
21) C. T. Trinh, Y. Nakagawa, K. O. Hara, R. Takabe, T. Suemasu, and N. Usami, Mater. Res. Express **3**, 076204 (2016).
22) K. Takahashi, Y. Nakagawa, K. O. Hara, I. Takahashi, Y. Kurokawa, and N. Usami, MRS Adv. **3**, 1435 (2018).

23) T. Yoshitake, A. Yuri, and K. Nagayama, Appl. Phys. Lett. 88, 182104 (2006).
24) S. Ogawa, A. Katagiri, T. Shimizu, M. Matsushima, K. Akiyama, Y. Kimura, H. Uchida, and H. Funakubo, J. Electron. Mater. 43, 2269 (2014).
25) S. Matsuno, R. Takabe, S. Yokoyama, K. Toko, M. Mesuda, H. Kuramochi, and T. Suemasu, Appl. Phys. Express **11**, 071401 (2018).
26) R. Takabe, T. Deng, K. Kodama, Y. Yamashita, T. Sato, K. Toko, and T. Suemasu, J. Appl. Phys **123**, 045703 (2018).
27) Y. Inomata, T. Nakamura, T. Suemasu, and F. Hasegawa, Jpn. J. Appl. Phys. **43**, L478 (2004).
28) K. O. Hara, C. T. Cham, Y. Kurokawa, K. Arimoto, J. Yamanaka, K. Nakagawa, and N. Usami, Thin Solid Films **636**, 546 (2017).
29) N. Hiroi, T. Suemasu, K. Takakura, N. Seki, and F. Hasegawa, Jpn. J. Appl. Phys. **40**, L1008 (2001).
30) R. Takabe, W. Du, K. Ito, H. Takeuchi, K. Toko, S. Ueda, A. Kimura, and T. Suemasu, J. Appl. Phys. **119**, 025306 (2016).
31) H. Hoshida, N. Murakoso, T. Suemasu, and Y. Terai, Defect and Diffusion Forum **386**, 43 (2018).
32) Y. Terai, H. Yamaguchi, H. Tsukamoto, N. Murakoso, M. Iinuma, and T. Suemasu, Jpn. J. Appl. Phys. **56**, 05DD02 (2017).
33) T. Motohiro and Y. Taga, Thin Solid Films **112**, 161 (1984).
34) Ar sputter yield values from National Physics Laboratory, UK. (http://www.npl.co.uk/upload/pdf/energy_density_sublim.pdf)
35) M. Kumar, N. Umezawa, W. Zhou, and M. Imai, J. Mater. Chem. A **5**, 25293 (2017).
36) D. Tsukahara, M. Baba, S. Honda, Y. Imai, K. O. Hara, N. Usami, K. Toko, J. H. Werner, and T. Suemasu, J. Appl. Phys. **116**, 123709 (2014).

Table I. Sample preparation detail; pressure (P), substrate temperature (T_S) during the sputtering, layer thickness (d), the number of plate-like Ba source on the target (N) are specified.

Sample	P (Pa)	T_S (°C)	d (nm)	N
A1	0.25	600	272	3
A2	0.4	600	230	3
A3	0.8	600	235	3
A4	1.0	600	220	3
A5	0.5/1.0	500/600	300	3

Fig. 1 GI-XRD patterns of samples A1-A6, sputtered at 600 °C on Si(111) substrates.

Fig. 2 Raman spectra of samples A1-A6, sputtered at 600 °C on Si(111) substrates.

Fig. 3 (a) Ba (red) and Si (black) atomic ratios as a function of P for the samples prepared without (dotted lines) and with one Ba source on the $BaSi_2$ target (solid lines). The broken lines are plotted as guides showing the Ba and Si atomic ratios of the $BaSi_2$ target. (b) Dependence of deposition rate of films sputtered at RT when only the $BaSi_2$ target is used. (a) and (b) are reproduced from Ref. 25.

Fig. 4 Photoresponse spectra of (a) samples A1-A4 and (b) samples A3 (one-step growth) and A5 (two-step growth), under V_{bias} = 0.5 V applied between the top and bottom electrodes.

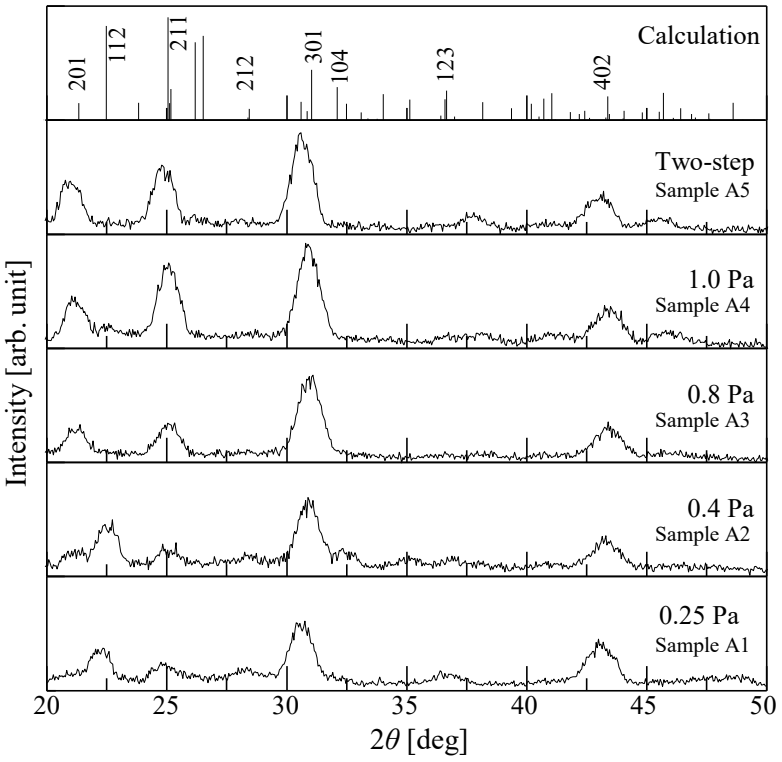
Calculation
201
112
211
212
301
104
123
402
Two-step
Sample A5
1.0 Pa
Sample A4
0.8 Pa
Sample A3
0.4 Pa
Sample A2
0.25 Pa
Sample A1
Intensity [arb. unit]
20
25
30
35
40
45
50
2θ [deg]

Fig. 1

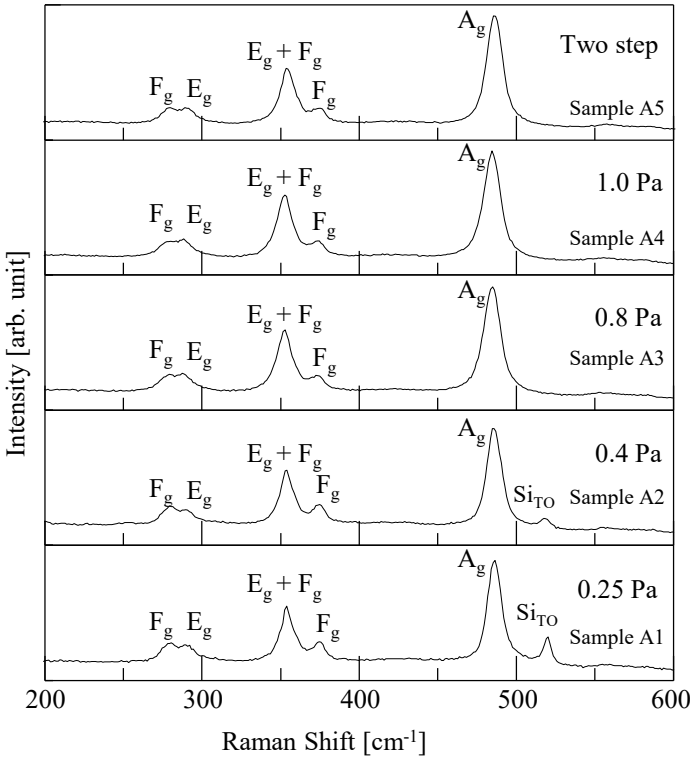
Intensity [arb. unit]
Raman Shift [cm-1]
200
300
400
500
600
Two step
Sample A5
1.0 Pa
Sample A4
0.8 Pa
Sample A3
0.4 Pa
Sample A2
0.25 Pa
Sample A1
Ag
Eg + Fg
Fg Eg
Fg
SiTO

Fig. 2

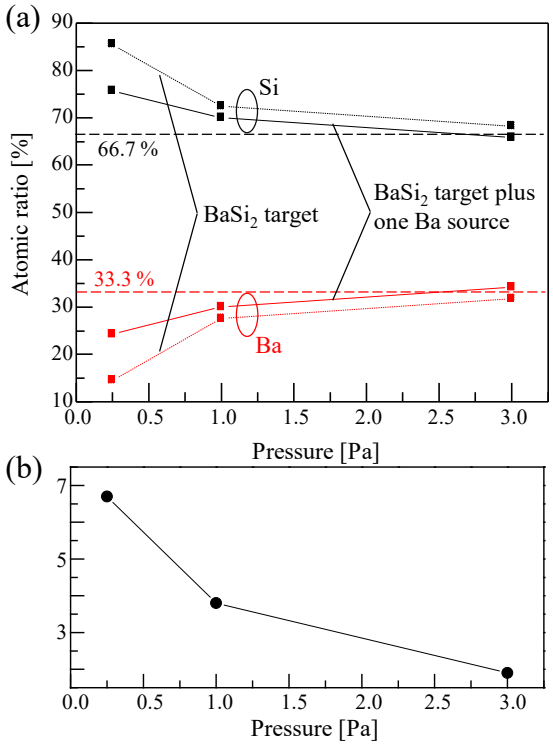
(a)
Atomic ratio [%]
Si
66.7 %
BaSi2 target
BaSi2 target plus
one Ba source
33.3 %
Ba
Pressure [Pa]
(b)
Pressure [Pa]

Fig. 3

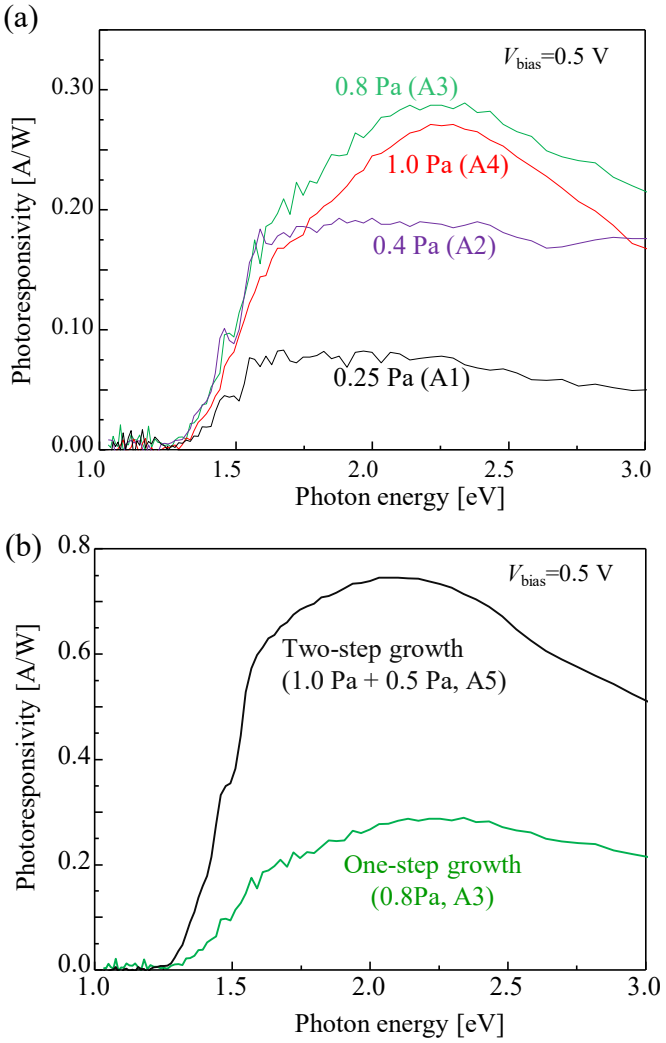
(a)
V_{bias}=0.5 V
0.8 Pa (A3)
1.0 Pa (A4)
0.4 Pa (A2)
0.25 Pa (A1)
Photoresponsivity [A/W]
Photon energy [eV]
(b)
V_{bias}=0.5 V
Two-step growth
(1.0 Pa + 0.5 Pa, A5)
One-step growth
(0.8Pa, A3)
Photoresponsivity [A/W]
Photon energy [eV]

Fig. 4